Available online at www.sciencedirect.com
SCIENCE DIRECT®
International Journal of Heat and Mass Transfer 47 (2004) 2927–2939
International Journal of HEAT and MASS TRANSFER
www.elsevier.com/locate/ijhmt

Thermal radiation in ultralight metal foams with open cells

C.Y. Zhao [1], T.J. Lu *, H.P. Hodson

Department of Engineering, University of Cambridge, Trumpington Street, Cambridge CB2 1PZ, UK

Received 13 June 2003; received in revised form 16 March 2004

Abstract

This paper presents results from experimental measurements on radiative transfer in FeCrAlY (a steel based high temperature alloy) foams having high porosity (95%) and different cell sizes, manufactured at low cost from the sintering route. The spectral transmittance and reflectance are measured at different infrared wavelengths ranging from 2.5 to 50 μm, which are subsequently used to determine the extinction coefficient and foam emissivity. The results show that the spectral quantities are strongly dependent on the wavelength, particularly in the short wavelength regime (<25 μm). Whilst the extinction coefficient decreases with increasing cell size, the effect of cell size on foam reflectance is not significant. When the temperature is increased, the total extinction coefficient increases but the total reflectance decreases. An analytical model based on geometric optics laws, diffraction theory and metal foam morphology is developed to predict the radiative transfer, with cell size (or cell ligament diameter) and porosity identified as the two key parameters that dictate the foam radiative properties. Close agreement between the predicted effective foam conductivity due to radiation alone and that measured is observed. At fixed porosity, the radiative conductivity of the metal foam increases with increasing cell size and temperature.

Keywords: Metal foams; Thermal radiation; Transmittance; Reflectance; Extinction coefficient; Emissivity; Experimental measurement; Modelling

1. Introduction

The transport of heat in highly porous, cellular metallic foams with open cells has been studied extensively in recent years [1–17]. The motivation is attributed to the high surface area to volume ratio as well as enhanced flow mixing due to the tortuosity of metal foams. Furthermore, metallic foams have attractive mechanical (e.g., stiffness, strength and energy absorption) and sound absorption properties [10], and can be processed in large quantity at low cost via the metal sintering route [13]. However, the focus of most previous studies has been placed on either the convective or conduction heat transfer at relatively low temperatures. Apart from low-temperature applications (e.g., compact heat exchangers for electronics cooling [1,10,13]), open-celled metal foams can also be used in high-temperature applications such as the porous radiant burner and acoustic liner in combustors [18,19]. For such high-temperature applications, radiation in metal foams is significant.

Zhao et al. [20] measured the effective thermal conductivity of one type of high temperature metal foam, FeCrAlY (Fe 73%, Cr 20%, Al 5%, Y 2%) foams, as a function of temperature in the range of 300–800 K under both atmospheric and vacuum conditions. The overall effect of thermal radiation on the whole thermal transport process (conduction, radiation and natural convection) for FeCrAlY foams having different cell sizes and porosities was quantified [20]. The results show that the contribution of radiative transfer (and natural convection [11]) increases significantly with increasing temperature, accounting for up to 50% of the effective (apparent) foam conductivity. Even though the contribution of natural convection can be excluded under

* Corresponding author. Tel.: +44-1223-766316; fax: +44-1223-332662.
E-mail address: tjl21@cam.ac.uk (T.J. Lu).
[1] Current address: Department of Mechanical Engineering, Brunel University, Uxbridge UB8 3PH, UK.

0017-9310/$ - see front matter © 2004 Elsevier Ltd. All rights reserved.
doi:10.1016/j.ijheatmasstransfer.2004.03.006

Nomenclature

C, C_1, C_2	constants
C_s	correction scan of source with sample
C_e	correction scan of source without sample
d_i	inner diameter of cell ligament, m
d_o	outer diameter of cell ligament, m
d_p	cell size, m
D_0	dark sample scan for zero offset
E	emissive power
f	influence function, Eq. (24)
I, I_λ	total intensity and spectral intensity of radiant energy
K, K_λ	total and spectral extinction coefficient, 1/m
K_R	Rosseland mean extinction coefficient, 1/m
K^*_λ	weighted spectral extinction coefficient, 1/m
k_c	effective thermal conductivity due to conduction, W/mK
k_e	effective thermal conductivity of metal foam, W/mK
k_r	effective radiative thermal conductivity, W/mK
L	sample height, m
m	complex refractive index
n	constant
q	heat flux, W/m^2
R_f	reference scan (hemisphere radiance)
S	sample scan (sample radiance)
T	temperature, K

Greek symbols

α, α_λ	absorption coefficient and spectral volume absorption coefficient
χ	non-dimensional size parameter
ε_{eff}	total emissivity
$\varepsilon_{\lambda,eff}$	spectral emissivity
λ	wavelength, m
ρ_{eff}	total reflectance
$\rho_{\lambda,eff}$	spectral reflectance
σ	Stefan–Boltzman constant
σ_s	scattering coefficient
τ, τ_λ	total transmittance and spectral transmittance
ϕ	porosity of foam
Φ_λ	spectral volumetric phase function of scattering

vacuum conditions, it is still difficult to isolate the thermal radiation effect from the effective conductivity measurements. Alternatively, by using analytical models of effective foam conductivity due to solid conduction alone [3,6,8], the radiation contribution can be obtained by subtracting the conduction part from the measured overall conductivity [2,20]. However, this is only an indirect method for studying radiation, which depends not only on the overall conductivity measurement but also on a reliable model of solid conduction in the metal foam. At present, there is little understanding on the real transfer mechanisms of radiation in metal foams.

In order to develop a theoretical model to predict the radiative properties of metal foams, the details of radiation must be investigated. The transport process of radiation in metal foams is complicated because of the complex cellular morphology and the inherent complexities associated with the transport mechanism itself. Although numerous studies on thermal radiation [21–34] have been carried out for polymer foams and fibrous insulations, little information can be found in the open literature on radiative heat transfer in metallic foams. Since metal foams have much higher effective solid conductivities ($k_c > 10$ W/mK) and larger diameters of cell ligaments ($d_o = 30$–800 m), in contrast with the commonly used thermal insulation foams ($k_c < 1$ W/mK and $d_o = 3$–20 μm), it is expected that their radiative properties will be considerably different from those of the insulation foams. Consequently, previous theoretical and experimental results on insulation foams are not (directly) applicable to metal foams.

The objective of the present study is to use a combined experimental and theoretical study to explore the radiation mechanisms in open-celled cellular metal foams. The metal foam will be considered as a semi-transparent medium capable of absorbing, emitting and scattering thermal radiation. The spectral transmittance and reflectance of FeCrAlY foams with different cell sizes but fixed porosity (~95%) will be measured over the temperature range of 300–800 K, and subsequently used to determine the spectral extinction coefficient as well as the total emissivity and extinction coefficient. The radiative conductivity deduced from the overall thermal conductivity measured with the guarded hot plate apparatus in vacuum will also be presented, and compared with the predictions from an analytical model built upon geometric optics laws, diffraction theory and metal foam morphology.

2. Metal foam samples

The microstructure of a typical cellular metal foam having open cells consists of ligaments forming a network of inter-connected dodecahedral-like cells, as shown in Fig. 1. The cells are randomly oriented, and

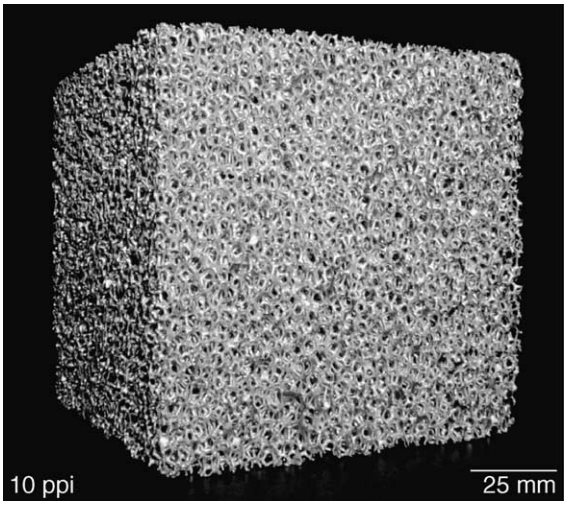

Fig. 1. FeCrAlY foam manufactured with the sintering route.

mostly homogeneous in size and shape. Pore size may be varied from approximately 0.2 to 7 mm. The relative density—defined as the ratio of the density of the foam to that of the solid of which the foam is made—can be varied from 3% to 15% (this can be further increased by compression if needed [7]). Alloys and single-element materials are available. Common materials include copper, aluminum, nickel, and steel. The distinctive feature of metal foams processed by the metal sintering technique is that the cell edge struts (ligaments) are hollow (Fig. 2) compared to the solid struts of metal foams manufactured via the more expensive investment casting route that are studied in [1–7].

A total of three FeCrAlY foam samples with a fixed porosity of 95% but different cell sizes—30, 60 and 90 ppi (pores per inch)—were produced via the sintering route and supplied by Porvair Fuel Cell Technology. Of the methods suitable for producing metal foams, the metal sintering method offers the most promise as a method that is capable of economically producing millions of components annually [13]. The process is similar to the production of ceramic foams that are used in molten metal filtration (and many other applications), except in the heat treatment process. Heat treatment needs, however, are identical to that required in powder metal industry for sintering pressed and injection molded materials, which are mass-produced routinely.

The specimens were cut to 5–10 mm of thickness for the spectral transmittance measurement and 25 mm for the spectral reflectance measurement by using the electrical discharge machine (EDM), which provides a good quality cutting section without damaging foam structures. For each sample, the ratio of its smallest overall dimension (thickness L) to its cell size is at least 10, and hence the sample can be considered as an effective porous medium. Specifications (ppi, cell size, relative density, width, length, height, etc.) of the foam samples tested are given in Table 1.

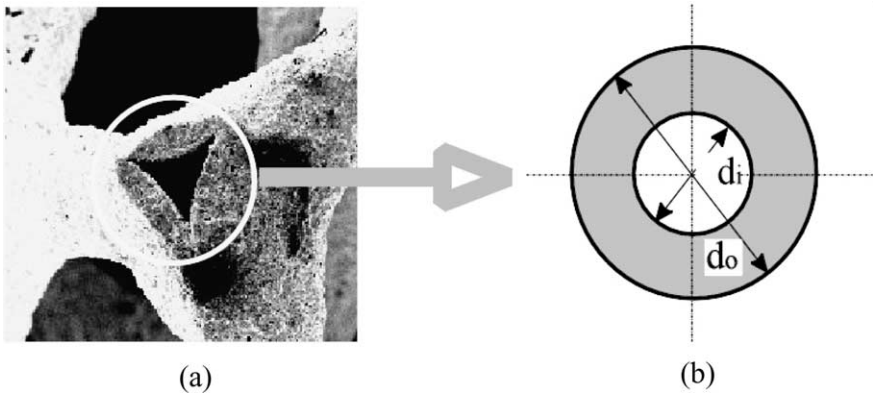

Fig. 2. (a) Typical hollow cell ligament and (b) cylindrical cell ligament and notations.

Table 1
Specifications of test samples

ppi (pores per inch)	30	60	90
Relative density (%)	5	5	5
Cell size (mm)	0.847	0.423	0.282
Dimension for transmittance: length × width × thickness (mm)	40 × 40 × 10	40 × 40 × 8	40 × 40 × 5
Dimension for reflectance: length × width × thickness (mm)	n.a.	40 × 40 × 25	40 × 40 × 25

3. Experimental equipment and measurement procedures

The spectral transmittance and reflectance were measured at NPL (National Physical Laboratory, UK). As shown in Fig. 3, the equipment consists of a Perkin-Elmer 580B spectrophotometer covering the infrared wavelength range from 2.5 to 50 μm, a reflectometer/transmissometer device and the associated cooling, purging and digital recording systems. The whole system was designed to fit in a large compartment. The essential principle of reflectance measurement is shown in Fig. 4. A 150 mm diameter hemispherical copper mirror in a gimbal mounting is used to focus radiation from a cylindrical ceramic source onto the neighboring sample so as to produce a uniform hemispherical irradiation. A small aperture only slightly larger than the cross section of the measuring beam is located centrally in the hemispherical mirror. A precision slide for the mounting bars of the reflectometer allows it to be moved sideways to reproducible positions that are adjustable with locked stop-screws. One position is the normal position, with the bars centrally aligned with the sample beam optical axis, so that the beam axis passes through the sample aperture. This allows the usual types of spectral scan to record hemisphere mirror radiance (Fig. 4a) and sample radiance (Fig. 4b). The other position is displaced 20 mm, so that the beam axis passes through the centre of the source. This allows the two extra types of scan to be made, with and without the presence of the sample (Fig. 4c and d), in order to consider the correction factor due to the inter-reflection effect between the source and the sample [35].

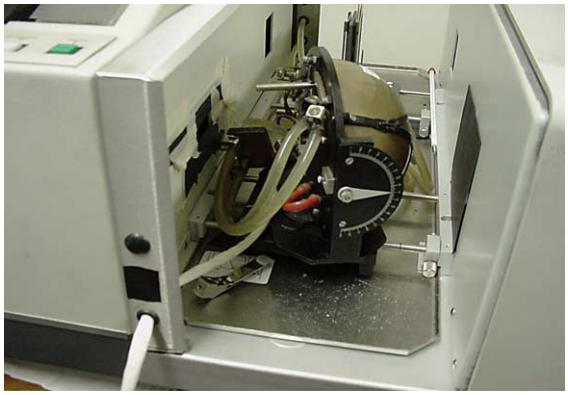

Fig. 3. Test facility for spectral transmittance and reflectance measurement.

A total of nine scans are made in the following sequence: R_f1, $S1$, C_s1, C_e1, D_0, C_e2, C_s2, $S2$, R_f2, where

R_f	reference scans (hemisphere radiance)
S	sample scans (sample radiance)
C_s	correction scans of source with sample
C_e	correction scans of source without sample
D_0	dark sample scan for zero offset

This sequence of scans is symmetrical with respect to time, and hence is likely to nullify most of the effects of instrumental drift. The spectral reflectance can then be obtained as

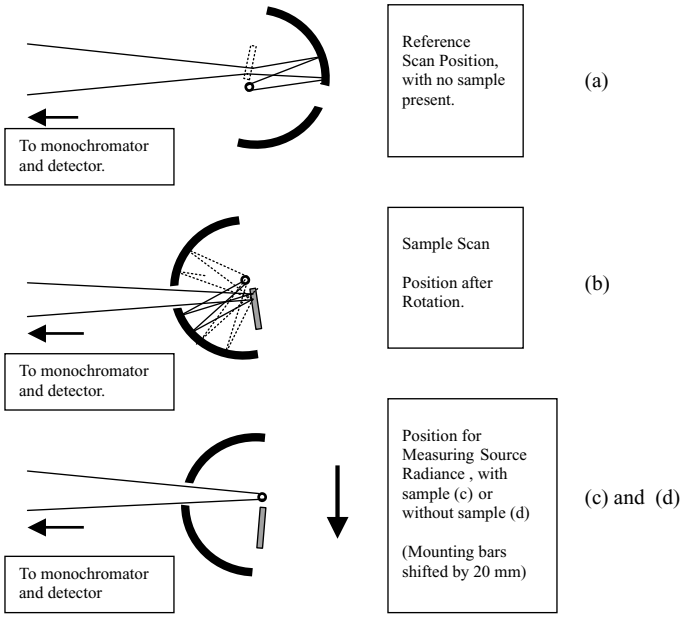

Fig. 4. Operating principle of hemispherical reflectometer/transmissometer.

$$\rho_{\lambda,\mathrm{eff}} = \frac{S1 + S2 - 2 \cdot D_0}{R_f 1 + R_f 2 - 2 \cdot D_0} \times \frac{C_e 1 + C_e 2 - 2D_0}{C_s 1 + C_s 2 - 2D_0} \quad (1)$$

where the first ratio is the usual apparent reflectance, while the second ratio is the correction factor for the inter-reflection effect between the heat source and sample [36].

For the transmittance measurement, the principle and procedures are identical to the reflectance measurement except that the hemisphere in Fig. 4b now turns around by 180°, in order for the radiance of the hemisphere to pass through the sample. The transmittance (τ_λ) is defined as the ratio of the thermal radiation intensity $I_\lambda(L)$ passing through the sample to the radiation intensity before the sample $I_\lambda(0)$:

$$\tau_\lambda = \frac{I_\lambda(L)}{I_\lambda(0)} \quad (2)$$

During the measurement, the spectrophotometer system is continuously purged of water vapor and carbon dioxide by means of a recirculating air purifier. In order to prevent local over-heating of the sample, the source is markedly under-run and its temperature is maintained at 950 K. For reflectance measurement, the sample is backed by a water-cooled copper block to enhance the heat dissipation, whilst for the transmittance measurement the sample is cooled by a stream of water-free N_2. Thus, for both measurements, the sample temperature is maintained at 30 ± 3 °C during the test. The infrared source is stabilized using a unique constant-load-resistance power supply that negates the effect of purging draught. The overall uncertainty of the measurement at the 95% confidence level is ±5% [35,36]. This mainly arises from the presence of the necessary viewing aperture, which causes the hemispherical irradiation of the sample to be less than that expected owing to the missing solid angle of the small aperture (Fig. 4).

4. Experimental results

4.1. Spectral transmittance, τ_λ

For black bodies, the monochromatic emissive power was derived by Planck by introducing the quantum concept for electromagnetic energy as

$$E_{b\lambda}(T,\lambda) = \frac{C_1 \lambda^{-5}}{e^{C_2/\lambda T} - 1} \quad (3)$$

where $C_1 = 3.743 \times 10^{-16}$ W m^2 and $C_2 = 1.4387 \times 10^{-2}$ mK. By integrating Eq. (3) over the wavelength, it has been established that over 90% of the thermal radiation lies in the wavelength range between 2.5 and 50 μm for a typical sample temperature of 800 K. Consequently, in the present study, the spectral quantities have all been measured for the wavelength range of 2.5–50 μm.

The measured transmittance is plotted as a function of wavelength in Fig. 5a–c for FeCrAlY foam specimens with a fixed relative density (5%) but different cell sizes (Table 1). The results of Fig. 5 demonstrate that the foam transmittance property is strongly dependent upon the spectral wavelength. The transmittance initially increases with increasing wavelength, reaching the first peak at around 18 μm, and then decreases somewhat before rising again sharply to the second peak at around

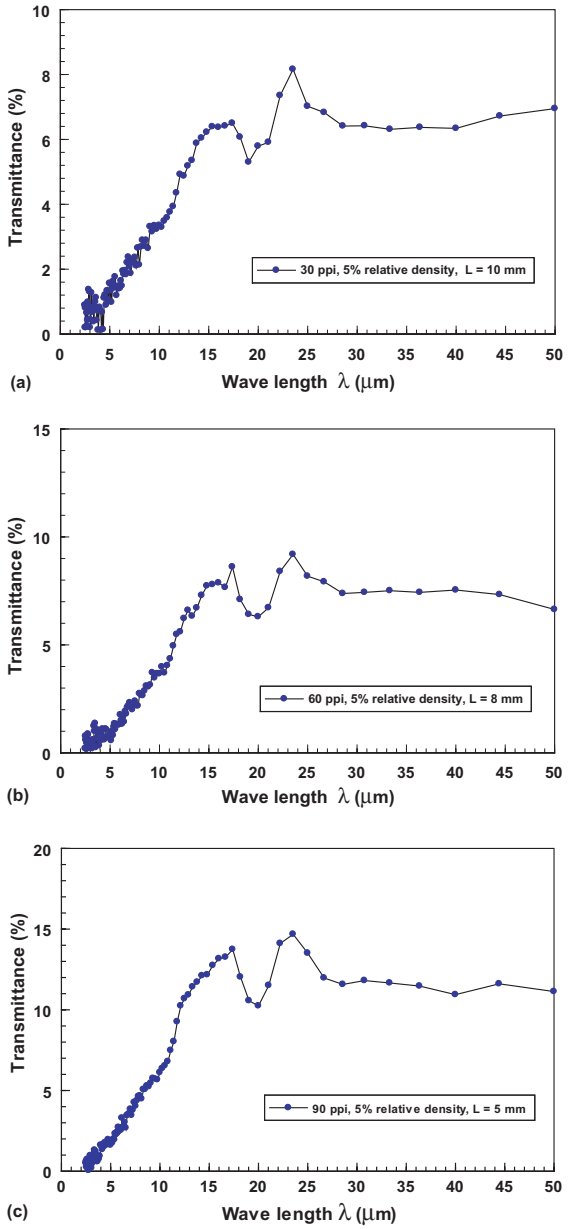

Fig. 5. Spectral transmittance of FeCrAlY foam with: (a) 30 ppi, (b) 60 ppi, and (c) 90 ppi.

25 μm; afterward the transmittance gradually decreases and reaches a plateau. It is noticed that the transmittance of all the three samples tested exhibit similar dependence upon of the wavelength. These samples have similar cellular structures and identical porosity (95%); the only difference is their cell size: 0.28, 0.42 and 0.85 mm (Table 1). This implies that the same thermal radiation mechanism is in force for these foams, with the transmittance versus wavelength relation determined mainly by the foam microstructures and solid material properties as long as the porosity is sufficiently large.

4.2. Extinction coefficient

As an overall quantity, the transmittance presented in Fig. 5 depends on the thickness of the foam sample. To study the thermal radiation within a foam, its local radiative property, the extinction coefficient K_λ, is needed. Physically, the extinction coefficient represents the decay rate of the radiation intensity passing through the material and, for a homogeneous isotropic foam, it should be independent of the sample thickness. It is therefore a more general and meaningful material property than the transmittance.

For radiant energy passing through a foam sample in its thickness direction (x-direction) at wavelength λ, the decrease of its intensity I_λ can be related to the extinction as

$$\frac{dI_\lambda}{dx} = -\alpha_\lambda I_\lambda - \sigma_{s\lambda} I_\lambda \equiv -K_\lambda I_\lambda \tag{4}$$

where α_λ and $\sigma_{s\lambda}$ are the absorption and scattering coefficient, respectively, their sum being the extinction coefficient, K_λ. Note that the self-emission by the foam and the anisotropic scattering effect are neglected in (4), as these are considered lesser effects in comparison with that due to extinction. From (4), the relationship between the transmittance and extinction can be obtained as

$$\tau_\lambda = \frac{I_\lambda(L)}{I_\lambda(0)} = e^{-K_\lambda L} \tag{5}$$

which, in turn, can be used to determine the spectral extinction coefficient as

$$K_\lambda = -\frac{\ln(I_\lambda(L)/I_\lambda(0))}{L} = -\frac{\ln(\tau_\lambda(L))}{L} \tag{6}$$

The spectral extinction coefficient calculated from (6) is presented in Fig. 6 as a function of wavelength for all the three samples. The extinction coefficient decreases sharply as the wavelength is increased to about 15 μm, and then maintains roughly at a constant level for wavelengths larger than 25 μm (Fig. 6). The value of K_λ at short wavelength (<5 μm) is approximately twice that at long wavelength (>25 μm). The results also show that

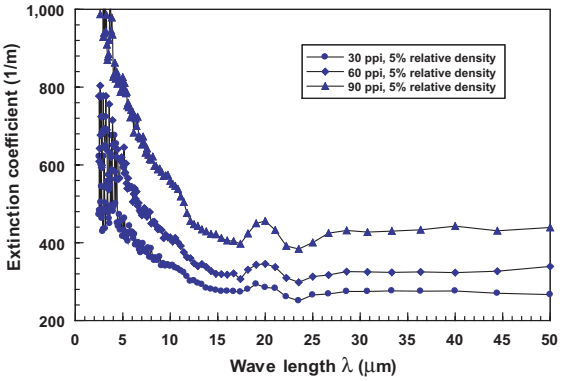

Fig. 6. Effect of cell size on spectral extinction coefficient plotted as a function of wavelength.

the extinction coefficient decreases with increasing cell size, from about 420 1/m at 30 μm wavelength for the 90 ppi sample to about 240 1/m at the same wavelength for the 30 ppi sample.

For engineering applications, the total extinction coefficient K is a more commonly used material parameter than the spectral extinction coefficient K_λ, as the former represents the overall effect of energy decay in the material. The total extinction coefficient is defined as

$$K = -\frac{\ln(I(L)/I(0))}{L} = -\frac{\ln(\tau(L))}{L} \tag{7}$$

where $I(L)$ and $I(0)$ are the total intensities (spectrally integrated) before and after the metal foam sample of thickness L, respectively, whilst τ is the total transmittance given by

$$\tau(L) = \frac{\int_0^\infty I_\lambda(L)\,d\lambda}{\int_0^\infty I_\lambda(0)\,d\lambda} = \frac{\int_0^\infty I_\lambda(0)\tau_\lambda\,d\lambda}{\int_0^\infty I_\lambda(0)\,d\lambda} \tag{8}$$

The radiation intensity emitted from the black body source is known [37]:

$$I_\lambda = \frac{E_{b\lambda}}{\pi} \tag{9}$$

where $E_{b\lambda}$ is the emissive power per unit wavelength, and is given by Eq. (3).

Given the fact that there is no obvious change in the physical and chemical properties of a FeCrAlY foam up to 600 °C, the spectral transmittance τ_λ measured at room temperature is assumed applicable for all the temperatures below 600 °C. However, the total transmittance τ does vary with temperature, due to the temperature dependence of the spectral intensity in accordance with Eq. (3). The total extinction coefficient K thus determined is plotted as a function of temperature in Fig. 7. That K

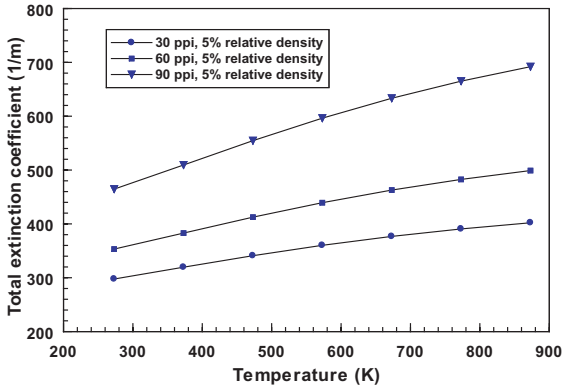

Fig. 7. Total extinction coefficient plotted as a function of temperature for foams with different cell sizes (at fixed relative density).

increases (nearly linearly) with increasing temperature (Fig. 7) can be explained by the fact that the proportion of thermal radiation at short wavelengths will increase with increasing temperature according to (3), and that the spectral extinction coefficient is larger for shorter wavelengths than that for the longer wavelengths, as shown in Fig. 6. The results of Fig. 7 also reveal that the total extinction coefficient decreases considerably with increasing cell size.

4.3. Reflectance

For applications where metal foams are used as a heat source, their external radiation property, the foam reflectance, needs to be known. The measured spectral foam reflectance $\rho_{\lambda,\mathrm{eff}}$ for two samples (60 and 90 ppi) is shown in Fig. 8. The thickness of both samples is 25 mm, which is sufficiently large to prevent the radiation passing through the sample. Fig. 8 shows that the spectral

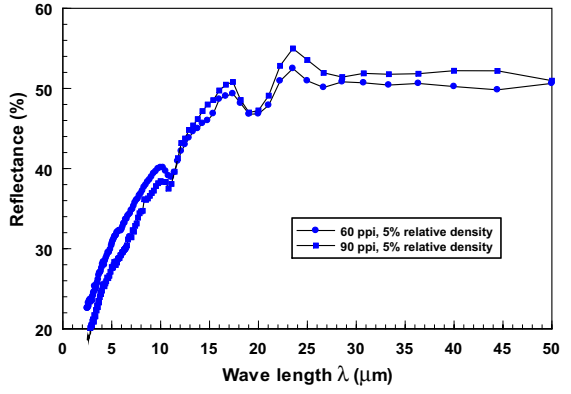

Fig. 8. Effect of cell size on spectral reflectance.

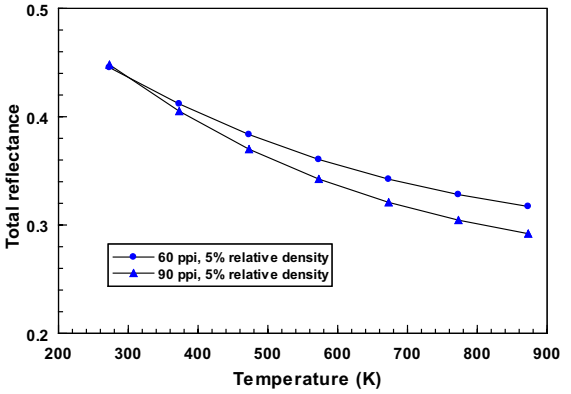

Fig. 9. Variation of total reflectance with temperature.

reflectance increases sharply with increasing wavelength until it reaches a plateau at a wavelength of about 25 μm, and the effect of cell size is small. This implies that the reflectance of the foam mainly depends on the surface properties of cell ligaments and cellular structures as long as the foam sample is sufficiently thick.

Similar to the total transmittance, the total reflectance is defined as

$$\rho_{\mathrm{eff}} = \frac{\int_0^\infty I_\lambda(0)\rho_{\lambda,\mathrm{eff}}\,\mathrm{d}\lambda}{\int_0^\infty I_\lambda(0)\,\mathrm{d}\lambda} \tag{10}$$

Fig. 9 shows the total reflectance plotted as a function of temperature for the two samples.

4.4. Emissivity

From the measured spectral reflectance, the spectral emissivity of a foam can be obtained as

$$\varepsilon_{\lambda,\mathrm{eff}} = 1 - \rho_{\lambda,\mathrm{eff}} \tag{11}$$

from which the commonly used total emissivity is calculated as

$$\varepsilon_{\mathrm{eff}} = \frac{\int_0^\infty I_\lambda(0)\varepsilon_{\lambda,\mathrm{eff}}\,\mathrm{d}\lambda}{\int_0^\infty I_\lambda(0)\,\mathrm{d}\lambda} = 1 - \rho_{\mathrm{eff}} \tag{12}$$

Fig. 10 plots $\varepsilon_{\mathrm{eff}}$ as a function of temperature for the two 60 and 90 ppi samples tested.

It is emphasized that the reflectance and emissivity presented hitherto refer to foam samples sufficiently thick (25 mm) such that the radiation cannot pass the sample. Also, the reflectance and emissivity thus measured are considered to be independent of sample thickness, because the associated radiation process occurs mainly at the foam surface and in the layers of cells close to the surface: the radiation away from the surface cannot be reflected outside the foam due to multiple reflecting and scattering within the foam.

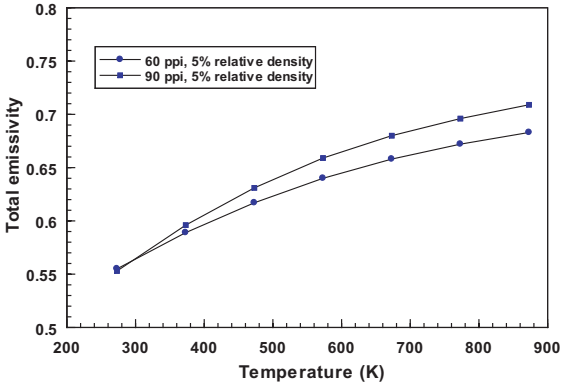

Fig. 10. Variation of total emissivity with temperature.

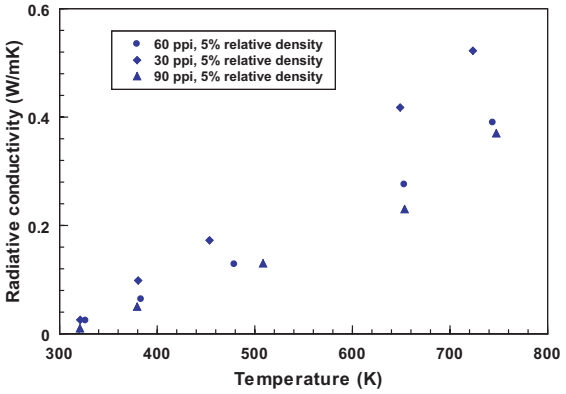

Fig. 11. Radiative conductivity plotted as a function of temperature for selected values of cell size at fixed relative density.

4.5. Effective radiative conductivity k_r

Apart from the radiative properties measured and discussed above, the overall effective thermal conductivity of FeCrAlY foams in the temperature range of 300–800 K has been separately measured with the guarded-hot-plate apparatus for both atmospheric and vacuum conditions [20]. Under vacuum conditions, the measured overall effective thermal conductivity, k_e, comprises two different heat transfer modes: solid conduction and thermal radiation.

For one-dimensional steady state heat transfer via the conduction and radiation routes across a metal foam in vacuum, the local heat flux averaged over a representative unit cell of the foam can be approximately written as

$$q = q_c + q_r = -(k_c + k_r)\frac{dT}{dx} = -k_e\frac{dT}{dx} \tag{13}$$

where q_c and q_r represent separately the conduction and radiation heat flux, and k_c and k_r are the corresponding effective thermal conductivity due to conduction and radiation, respectively.

Analytical formulations for the effective solid conductivity, k_c, of metal foams can be found in many papers, e.g., [6,8,20]. Models on their effective radiative conductivity, k_r, will be given in the next section by using the volume averaging, continuous effective medium approach, and in a companion paper [38] by using the non-continuous medium (periodic unit cell) approach. On the other hand, the radiative conductivity can also be obtained by subtracting the predicted conduction conductivity k_c using analytical models [6,8,20] from the measured overall thermal conductivity k_e [20]. The radiative conductivity deduced in this way is plotted as a function of temperature in Fig. 11 for the three samples listed in Table 1. The results show that k_r increases as the cell size or temperature is increased. In general, the extinction coefficient (the sum of the absorption and scattering coefficients) decreases with increasing cell size, and hence the corresponding "penetration thickness" is larger than that associated with smaller cell sizes. Larger "penetration thickness" implies that more heat can be directly transferred via radiation to deeper locations of the foam sample, resulting in a higher radiative conductivity as the cell size is increased.

5. Modeling based on the effective medium approach

For simplicity, the metal foam will be considered as a semi-transparent, isotropic, effective medium capable of absorbing, emitting, and scattering thermal radiation. In principle, the calculation of combined radiation and conduction in such a medium can be carried out by using the radiation transfer equation in conjunction with the energy conservation equation. In practice, however, the strict form of the radiation transfer equation is often not used due to its extreme complexity. Existing models for semi-transparent media are primarily based on either the two-flux approach or the diffusion approximation utilizing the Rosseland mean coefficient.

Tong and Tien [21,22] and Lee [23–25] used the two-flux model to study thermal transport in fibrous insulations, assuming that the intensity of radiation in the forward and backward directions can be represented by two different but isotropic components. More recently, Doermann and Sacadura [26], Baillis et al. [27,28], Glicksman et al. [29,30], Kuhn et al. [31], Lee and Cunnington [32,33] and Caps et al. [34], amongst others, modelled thermal radiation in fibrous insulations by using a diffusion approximation based on a combination of the geometric optics laws and diffraction theory. Since the latter approach can provide a better prediction and clearer physical understanding on thermal radiation in metal foams, it will be employed below. Furthermore, metal foams are in general optically sufficiently thick enough to satisfy the conditions of using this approach.

The application of the diffusion-based method requires the knowledge of three radiative properties: absorption coefficient, scattering coefficient and phase function. Mie [39] applied the electromagnetic theory to derive these radiative properties based on the assumption of independent interaction of thermal radiation with individual particles when a plane monochromatic wave is incident upon a spherical surface. Using the Mie theory, Van de Hulst [40] examined the limiting cases for very small and very large particles. However, for the metal foams studied in this paper, the individual cell ligaments (Fig. 2) are joined together at the junctions, so there is no reason to assume the single independent scattering. Moreover, the presence of impurities and any specially introduced alloy element additions for sintering enhancement may change noticeably the radiative properties. Consequently, it is unlikely that satisfactory predictions can be obtained with the Mie theory for metal foams. In the following, an analytical model based on the geometric optics laws, diffraction theory and metal foam morphology will be constructed to predict the foam radiative properties (absorption, scattering and phase function) and heat transfer.

5.1. Rosseland diffusion

As shown in Eq. (13), if the temperature gradient is sufficiently small or the optical thickness is sufficiently large, the local radiative heat flux mainly depends on the local temperature gradient, and hence can be written in a way similar to the diffusion-controlled Fourier conduction as

$$q_r = -k_r \frac{dT}{dy} \tag{14}$$

The proposed formulation of the (effective) radiative conductivity k_r is based on a modified diffusion approximation that accounts for scattering by the porous (fibrous) medium. If the thickness of the foam sample is large enough for it to be optically thick, its radiative conductivity can be approximated by the Rosseland equation [26–34] as

$$k_r = \frac{16\sigma T^3}{3K_R} \tag{15}$$

where K_R is the Rosseland mean extinction coefficient defined by

$$\frac{1}{K_R} = \int_0^\infty \frac{1}{K_\lambda} \frac{dE_{b\lambda}(T,\lambda)}{dE_b(T)} d\lambda \tag{16}$$

Here, $E_{b\lambda}$ and E_b are the spectral and total emissive power of a blackbody, respectively, with $E_{b\lambda}$ already given in Eq. (3). The total radiation E_b is obtained by integrating Eq. (3) over all wavelengths:

$$E_b(T) = \sigma T^4 \tag{17}$$

where $\sigma = 5.669 \times 10^{-8}$ W/m^2 K^4 is the Stefan–Boltzmann constant.

The Rosseland equation is valid when the medium absorbs and scatters isotropically [41]. However, scattering measurements by Glicksman et al. [29] have shown that scattering by insulation foams that have cellular morphologies similar to those of the metal foams studied here is highly anisotropic. A weighted spectral extinction coefficient K_λ^* has thence been suggested to account for anisotropic scattering [41,42] in place of K_λ in Eq. (16) as

$$K_\lambda^* = \alpha_\lambda + \sigma_{s\lambda}^* \tag{18}$$

where α_λ is the spectral volumetric absorption coefficient, and $\sigma_{s\lambda}^*$ is the weighted scattering coefficient, given by

$$\sigma_{s\lambda}^* = \sigma_{s\lambda}(1 - \langle \cos\theta \rangle_\lambda) \tag{19}$$

with

$$\langle \cos\theta \rangle_\lambda = 0.5 \int_{-1}^{1} \Phi_\lambda(\theta) \cos\theta \, d(\cos\theta) \tag{20}$$

Here, $\sigma_{s\lambda}$ is the spectral volumetric scattering coefficient, whereas $\Phi_\lambda(\theta)$ is the spectral volumetric phase function of scattering that has the physical interpretation of being the scattered intensity in one direction, divided by the intensity that would be scattered in this direction if the scattering was isotropic.

In order to determine the weighted extinction coefficient K_λ^*, three parameters need to be known, namely, spectral absorption coefficient α_λ, spectral scattering coefficient $\sigma_{s\lambda}$ and phase function of scattering $\Phi_\lambda(\theta)$. As a result, the remaining task is how to make use of the measured radiative properties presented in the previous section to formulate the three parameters in terms of foam morphological parameters and optical properties of the solid material of which the foam is made.

5.2. Spectral absorption and scattering coefficients

The absorption and scattering of heat in a metal foam is governed by electromagnetic field equations and the associated boundary conditions at all interfaces, and can be explained by local reflection, refraction, and diffraction. When a thermal radiation wave strikes the surface of a cell strut (Fig. 2), a portion of it is reflected, while the remainder penetrates into the strut. The radiation wave within the strut may experience some absorption and multiple internal reflections before it escapes out of the strut in different directions, giving rise to scattering. This scattering process is the contribution by refraction. The diffraction scattering process originates from the bending of the incident radiation wave near the edge of the strut.

The scattering and absorption characteristics of a metal foam are essentially determined by five factors: foam morphology, porosity, strut shape, strut size relative to the wavelength of the incident radiation, and optical properties of the strut material. The cellular morphology of FeCrAlY foams and their porosity levels have been studied by Zhao and coworkers [8–10], and it has been assumed that the hollow triangular cell strut can be replaced by an equivalent cylinder of external diameter d_o and internal diameter d_i. The fourth factor is commonly expressed as a non-dimensional size parameter $\chi \equiv \pi d_o/\lambda$. The last factor is designated by the complex refractive index m. For most metals, the refractive index has large values at wavelengths longer than those in the visible regime; for example, $m = 1.87 + 21.3i$ for copper and $m = 1.51 + 1.63i$ for iron. The solutions of the electromagnetic fields are usually expressed in the form of an infinite series or complicated function of the aforementioned parameters. However, simple expressions exist for some limiting cases. The first of these is the small size limit or Rayleigh limit, $\chi \ll 1$ [43,44]. The second is the large size or geometric limit, $\chi \gg 1$.

The steel alloy foam studied in this paper can be used in the temperature range between room temperature and 1000 °C. The corresponding wavelength varies between 0.5 and 30 μm, whereas the cell strut diameter is typically in the range of 60–350 μm [8–10]. As a result, the size parameter χ is in general larger than 10, allowing the present study to focus on the geometric limit case. Under such conditions, the radiative properties are mainly dependent on the foam morphology, porosity and optical properties of the strut material. Also, from the measured results and the underlying physics of thermal radiation, it is known that the extinction coefficient increases in magnitude with decreasing cell size and increasing relative density.

Consequently, the proposed model for predicting the foam radiative properties is based on two independent parameters—porosity ϕ and strut diameter d_o (or pore size d_p)—that characterise the foam morphology as

$$\sigma_{s\lambda} = C(\rho_\lambda + 1)\frac{(1-\phi)^n}{2d_o} \tag{21}$$

$$\alpha_\lambda = C(1-\rho_\lambda)\frac{(1-\phi)^n}{2d_o} \tag{22}$$

The extinction coefficient then becomes:

$$K_\lambda = \sigma_{s\lambda} + \alpha_\lambda = C\frac{(1-\phi)^n}{d_o} \tag{23}$$

Here, C and n are material constants to be determined, and ρ_λ is the spectral reflectivity of the solid material. In the present study, the strut material is assumed grey and $\rho_\lambda \approx 0.6$ for steel [37]. Note that the radiative model proposed by Tien [45] for packed beds can be recovered by setting $C = 3$ and $n = 1$ in Eqs. (21)–(23) and assuming that the solid material is opaque and grey, with $\rho_\lambda = \rho = 1 - \alpha = 1 - \varepsilon$.

For FeCrAlY foams, the constants C and n are determined by using the measured spectral extinction coefficient, as follows. Firstly, it is noticed that whilst the predicted extinction coefficient of Eq. (23) is independent of wavelength λ, the measurements shown in Fig. 6 reveal a strong wavelength dependence. To account for this spectral dependence and hence to match the model predictions with the measured spectral extinctions (Fig. 6), the following influence function is proposed to be used in conjunction with Eqs. (21)–(23):

$$f(\lambda) = \begin{cases} 1 + e^{-2.4\times10^5(\lambda - 2.5\times10^{-6})}, & \lambda \geqslant 2.5\times10^{-6}\ \text{m}, \\ 2, & \lambda < 2.5\times10^{-6}\ \text{m} \end{cases} \tag{24}$$

Secondly, the cross-relationship between the strut diameter d_o and pore size d_p for FeCrAlY foams has been established via image analysis as [4,8–10]:

$$\frac{d_o}{d_p} = 1.18\sqrt{\frac{1-\phi}{3\pi}}\left(\frac{1}{1-e^{-((1-\phi)/0.04)}}\right) \tag{25}$$

In comparison with the strut diameter d_o, the pore (cell) size d_p is much easier to measure and also more commonly used in industrial product specifications, and hence d_p will be used instead of d_o below. Substituting (25) into (21)–(23) and then multiplying the right hand side of each equation by the influence function $f(\lambda)$, one obtains:

$$\sigma_{s\lambda} = \frac{C}{0.38}\left(1 - e^{-(1-\phi)/0.04}\right)(\rho_\lambda + 1) \times \frac{(1-\phi)^{n-0.5}}{2d_p} f(\lambda) \tag{26}$$

$$\alpha_\lambda = \frac{C}{0.38}\left(1 - e^{-(1-\phi)/0.04}\right)(1-\rho_\lambda) \times \frac{(1-\phi)^{n-0.5}}{2d_p} f(\lambda) \tag{27}$$

$$K_\lambda = \frac{C}{0.38}\left(1 - e^{-(1-\phi)/0.04}\right)\frac{(1-\phi)^{n-0.5}}{d_p} f(\lambda) \tag{28}$$

Finally, the constants C and n are determined by matching the predicted spectral extinction coefficients from (28) with those measured, as shown in Fig. 12. It is found that $n = 1$ for all the three samples tested, and $C = 0.445$, 0.278 and 0.30 for the 30, 60 and 90 ppi foam sample, respectively.

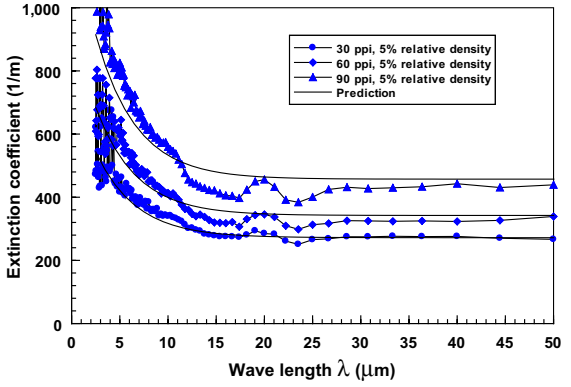

Fig. 12. Matching predictions with test data for spectral extinction coefficient.

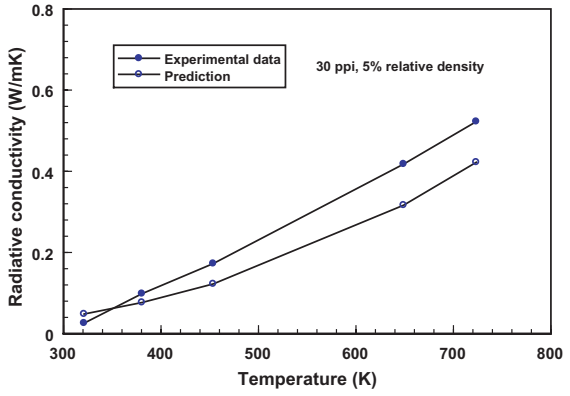

Fig. 13. Comparison between predicted and measured radiative conductivity for 30 ppi foam sample.

5.3. Phase function

When the strut size is much larger than the wavelength ($\chi \gg 1$) and the refractive index not very small ($m = 1.51 + 1.63\mathrm{i}$ for iron), which is the case of the studied metal foam, the geometric optics in conjunction with the diffraction theory can be used to predict the phase function of scattering $\Phi_\lambda(\theta)$. According to Brewster [46], $\chi = 5$ is the lowest value for which the phase function predicted by geometric optics combined with the diffraction theory can match reasonably well with that derived from the Mie theory. For open-celled polymer foams, this approach results in [26]:

$$\Phi_\lambda(\theta) = \frac{\rho_\lambda \Phi_{\mathrm{r}\lambda}(\theta) + \Phi_{\mathrm{d}\lambda}(\theta)}{1 + \rho_\lambda} \tag{29}$$

where $\Phi_{\mathrm{r}\lambda}(\theta)$ and $\Phi_{\mathrm{d}\lambda}(\theta)$ are the spectral phase function due to reflection and diffraction, respectively.

Since the phase function due to diffraction is extremely complicated and its effect on foam radiative properties has been found to be negligibly small [26], it will not be considered in the present study. For large opaque particles considered here, the phase function due to diffuse reflection is proposed [40,46]:

$$\Phi_\lambda(\theta) = \frac{8}{3\pi}(\sin\theta - \theta\cos\theta) \tag{30}$$

5.4. Prediction versus measurement

Once the spectral absorption coefficient, the spectral scattering coefficient and the phase function are known for a metal foam, its radiative conductivity k_r and other associated radiative properties can be obtained by solving Eqs. (15)–(20) and (26)–(30). The predicted results for the three FeCrAlY foam samples with different cell sizes but fixed porosity are shown in Figs. 13–15, and compared with those measured with the guarded hot plate apparatus in vacuum [20]. Whilst for the 60 ppi sample the agreement is very good, the predicted

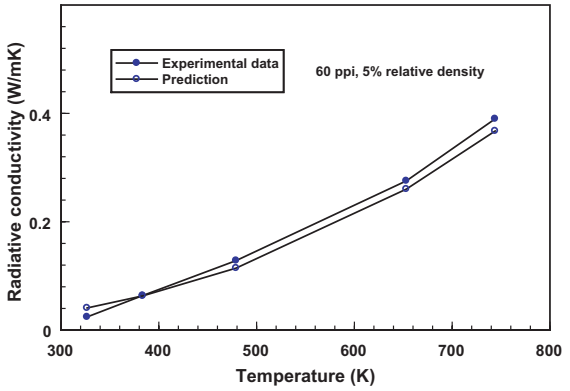

Fig. 14. Comparison between predicted and measured radiative conductivity for 60 ppi foam sample.

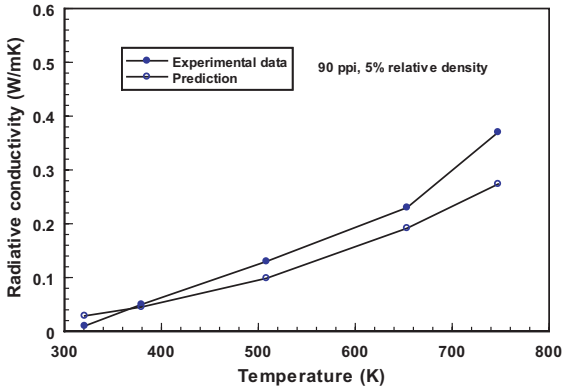

Fig. 15. Comparison between predicted and measured radiative conductivity for 90 ppi foam sample.

radiative conductivity is approximately twenty percent smaller than that measured for the other two samples. Given the complexity of thermal radiation in cellular foams and the various assumptions made in the present analytical modeling, the agreement between theory and experiment is considered reasonable.

6. Conclusions

The spectral transmittance and reflectance of highly porous steel alloy foams with open cells have been measured, which are then used to determine the extinction coefficient and emissivity. It is found that the spectral quantities are strongly dependent on the wavelength, particularly in the short wavelength regime (<25 μm). With the porosity fixed at 95%, the extinction coefficient of the foam decreases with increasing cell size, and its total extinction coefficient increases as the temperature is increased. The cell size has only a small effect on the foam reflectance, whilst the total reflectance decreases with increasing temperature. The radiative conductivity of the metal foam is obtained by first measuring its overall thermal conductivity in vacuum with the guarded hot plate apparatus, and then using results from analytical modeling to exclude the effect of solid conduction. With the porosity fixed, the radiative conductivity is found to increase with increasing cell size and increasing temperature. Based on the Rosseland diffusion equation and the metal foam microstructure, an analytical model has been developed to predict the foam conductivity due to thermal radiation alone. The prediction is compared with that measured, and satisfactory agreement has been obtained.

Acknowledgements

This work is supported partly by the US Office of Naval Research (ONR/ONRIFO grant number N000-140110271, and ONR grant number N000140210117), and partly by the UK Engineering and Physical Sciences Research Council (EPSRC grant number EJA/U83). The authors would like to thank Porvair Fuel Cell Technology for providing the FeCrAlY foam samples.

References

[1] T.J. Lu, H.A. Stone, M.F. Ashby, Heat transfer in open-celled metal foams, Acta Mater. 46 (1998) 3619–3635.
[2] T.J. Lu, C. Chen, Thermal transport and fire retardance properties of cellular aluminium alloys, Acta Mater. 47 (1999) 1469–1485.
[3] V.V. Calmidi, R.L. Mahajan, The effective thermal conductivity of high porosity fibrous metal foams, ASME J. Heat Transfer 121 (1999) 466–471.
[4] V.V. Calmidi, R.L. Mahajan, Forced convection in high porosity metal foams, ASME J. Heat Transfer 122 (2000) 557–565.
[5] J.W. Paek, B.H. Kang, S.Y. Kim, J.M. Hyun, Effective thermal conductivity and permeability of aluminium foam materials, Int. J. Thermophys. 21 (2000) 453–464.
[6] K. Boomsma, D. Poulikakos, On the effective thermal conductivity of a three-dimensionally structured fluid-saturated metal foam, Int. J. Heat Mass Transfer 44 (2001) 827–836.
[7] K. Boomsma, D. Poulikakos, The effects of compression and pore size variations on the liquid flow characteristics in metal foams, Trans. ASME J. Fluid Eng. 124 (2002) 263–272.
[8] C.Y. Zhao, T. Kim, T.J. Lu, H.P. Hodson, Modelling on thermal transport in cellular metal foams, in: 8th Joint AIAA/ASME Thermophysics and Heat Transfer Conference, AIAA 2002-3014, St. Louis, Missouri, USA, June 2002.
[9] C.Y. Zhao, T. Kim, T.J. Lu, H.P. Hodson, Thermal transport in high porosity cellular metal foams, J. Thermophys. Heat Transfer, in press.
[10] T.J. Lu, Ultralight porous metals: from fundamentals to applications, Acta Mech. Sinica 18 (2002) 457–479.
[11] A.G. Evans, J.W. Hutchinson, M.F. Ashby, Multifunctionality of cellular metal systems, Prog. Mater. Sci. 43 (1999) 171–221.
[12] T. Kim, A.J. Fuller, H.P. Hodson, T.J. Lu, An experimental study on thermal transport in lightweight metal foams at high Reynolds numbers, in: Proc. International Symposium of Compact Heat Exchangers, Grenoble, France, 2002, pp. 227–232.
[13] D. Haack, K. Butcher, T. Kim, H.P. Hodson, T.J. Lu, Novel lightweight metal foam heat exchanger, in: ASME International Mechanical Engineering Congress and Exposition, Proceedings V.3 (PID-4B: Heat Exchangers Applications for Change of Phase Media and Fuel Cells Systems, Book No. I00548), New York, 2001.
[14] M.L. Hunt, C.L. Tien, Effects of thermal dispersion on forced convection in fibrous media, Int. J. Heat Mass Transfer 31 (1988) 301–309.
[15] L.B. Younis, R. Viskanta, Experimental determination of the volumetric heat transfer coefficient between stream of air and ceramic foam, Int. J. Heat Mass Transfer 36 (1993) 1425–1434.
[16] Y.C. Lee, W. Zhang, H. Xie, R.L. Mahajan, Cooling of a FCHIP package with 100 w, 1 cm^2 chip, in: Proc. of the 1993 ASME Int. Elec. Packaging Conf., vol. 1, ASME, New York, 1993, pp. 419–423.
[17] S.Y. Kim, J.W. Paek, B.H. Kang, Flow and heat transfer correlations for porous fin in a plate-fin heat exchanger, J. Heat Transfer 122 (2000) 572–578.
[18] S.B. Sathe, R.E. Peck, T.W. Tong, A numerical analysis of heat transfer and combustion in porous radiant burners, Int. J. Heat Mass Transfer 33 (6) (1990) 1331–1338.
[19] T.W. Tong, S.B. Sathe, R.E. Peck, Improving the performance of porous radiant burners through use of sub-

micron size fibers, Int. J. Heat Mass Transfer 33 (6) (1990) 1339–1346.
[20] C.Y. Zhao, T.J. Lu, H.P. Hodson, J.D. Jackson, The temperature dependence of effective thermal conductivity of open-celled steel alloy foams, Mater. Sci. Eng. A367 (2004) 123–131.
[21] T.W. Tong, C.L. Tien, Analytical models for thermal radiation in fibrous media, J. Therm. Insul. 4 (1980) 27–44.
[22] T.W. Tong, C.L. Tien, Radiative transfer in fibrous insulations—Part I: Insulation study, J. Heat Transfer 105 (1) (1983) 70–75.
[23] S.C. Lee, Radiative transfer through a fibrous medium: allowance for fiber orientation, J. Quant. Spectrosc. Radiat. Transfer 36 (3) (1986) 253–263.
[24] S.C. Lee, Radiation heat transfer model for fibers oriented parallel to diffuse boundaries, J. Thermophys. Heat Transfer 2 (4) (1988) 303–308.
[25] S.C. Lee, Effect of fiber orientation on thermal radiation in fibrous media, Int. J. Heat Mass Transfer 32 (2) (1989) 311–319.
[26] D. Doermann, J.F. Sacadura, Heat transfer in open cell foam insulation, J. Heat Transfer 118 (1996) 88–93.
[27] D. Baillis, M. Raynaud, J.F. Sacadura, Spectral radiative properties of open-cell foam insulation, J. Thermophys. Heat Transfer 13 (3) (1999) 292–298.
[28] D. Baillis, M. Raynaud, J.F. Sacadura, Determination of spectral radiative properties of open cell foam: model validation, J. Thermophys. Heat Transfer 14 (2) (2000) 137–143.
[29] L.R. Glicksman, M. Schuetz, M. Sinofsky, Radiation heat transfer in foam insulation, Int. J. Heat Mass Transfer 30 (1) (1987) 187–197.
[30] L.R. Glicksman, A.L. Marge, J.D. Moreno, Radiation heat transfer in cellular foam insulation, Dev. Radiat. Heat Transfer, ASME HTD 203 (1992) 45–54.
[31] J. Kuhn, H.P. Ebert, M.C. Arduini-Schuster, D. Buttner, J. Fricke, Thermal transport in polystyrene and polyurethane foam insulations, Int. J. Heat Mass Transfer 35 (7) (1992) 1795–1801.
[32] S.C. Lee, G.R. Cunnington, Heat transfer in fibrous insulations: comparison of theory and experiment, J. Thermophys. Heat Transfer 12 (3) (1998) 297–303.
[33] S.C. Lee, G.R. Cunnington, Conduction and radiation heat transfer in high-porosity fiber thermal insulation, J. Thermophys. Heat Transfer 14 (2) (2000) 121–136.
[34] R. Caps, U. Heinemann, J. Fricke, Thermal conductivity of polyimide foams, Int. J. Heat Mass Transfer 40 (2) (1997) 269–280.
[35] F.J.J. Clarke, J.A. Larkin, Measurement of total reflectance, transmittance and emissivity over the thermal IR spectrum, Infrared Phys. 25 (1/2) (1985) 359–367.
[36] C.J. Chunnilall, F.J.J. Clarke, M.J. Shaw, Diffuse reflectance scales at NPL, in preparation.
[37] R. Siegel, J.R. Howell, Thermal Radiative Heat Transfer, third ed., Hemisphere Publishing, Washington, DC, 1992.
[38] C.Y. Zhao, T.J. Lu, H.P. Hodson, An analytical model for thermal radiation in open-celled metal foams, in preparation.
[39] G. Mie, Optics of turbid media, Ann. Phys. 25 (3) (1908) 377–445.
[40] H.C. Van de Hulst, Light Scattering by Small Particles, Wiley, New York, 1957, pp. 103–113.
[41] H.C. Hottel, A.F. Sarofim, Radiative Transfer, McGraw-Hill, New York, 1967, pp. 378–407.
[42] H. Lee, R.O. Buckius, Scaling anisotropic scattering in radiation heat transfer for a planar medium, J. Heat Transfer 104 (1982) 68–75.
[43] C.F. Bohren, D.R. Huffman, Absorption and Scattering of Light by Small Particles, Wiley, New York, 1983.
[44] M. Kerker, The Scattering of Light and Other Electromagnetic Radiation, Academic Press, New York, 1961.
[45] C.L. Tien, Thermal radiation in packed and fluidised beds, J. Heat Transfer 110 (1988) 1230–1242.
[46] M.O. Brewster, Thermal Radiative Transfer and Properties, Wiley, New York, 1992, pp. 301–336.